ELSEVIER

Materials Science and Engineering B37 (1996) 101–107

MATERIALS SCIENCE & ENGINEERING B

HREM simulations of particles and interfaces refined by molecular dynamics relaxations

Dirk Timpel, Kurt Scheerschmidt, Sergej Ruvimov[1]

Max Planck Institute of Microstructure Physics, 06120 Halle, Germany

Abstract

Precipitates in glasses as well as multi-layer semiconductor structures (quantum wells) are investigated by high resolution electron microscopy (HREM) providing local atomic information at the relaxed interfaces. The analysis of micrographs requires the computer simulation of the HREM contrast using a theoretical atomic structure model of the interfaces generated by molecular dynamics to describe the relaxations.

Keywords: Quantum wells; High resolution electron microscopy; Interfaces; Molecular dynamics

1. Introduction

Interfaces have a strong influence on material properties because they are associated with mechanical, chemical, and electrical inhomogeneities. Two different types of interface were investigated by high resolution electron microscopy (HREM) to discuss the relevance of the molecular dynamics (MD) model generation to the structure analysis applying HREM image simulations. First, silver particles in sodium silicate glasses are investigated. They are generated after sodium–silver ion exchange, thermally activated migration and subsequent annealing [1–3]. Second, HREM imaging will be discussed concerning multi-layer structures in the binary and ternary systems based on GaAs and GaSb [4–6].

2. HREM imaging and MD structure modelling

HREM, widely used in materials science, provides direct information on the local structural variability at the atomic level. However, a direct and phenomenological interpretation of the HREM micrographs is mostly not possible so that image processing and image simulations using theoretical structure models are inevitable. The HREM image contrast is mainly determined by two processes: first, by the electron interferences owing to the interaction process of the electron beam with the almost periodic potential of the matter, and second, by the interference of the plane waves scattered by the specimen and transferred by the microscope. Images are modelled by calculating both processes. Starting from an initial model, imaging conditions and model have to be varied up to a sufficient coincidence of simulated image and experimental contrast (trial and error).

Starting from geometrical models the relaxed structures were calculated by MD calculations and energy minimization mainly using the CERIUS program package [7]. Different force fields, consisting of simple two-, three-, and four-body potentials, i.e. distance, angle, torsion, and inversion of the bonds with respective parameters varied, were used to calculate the energy of a certain configuration. Some of the structures were refined by the program package of the Rutgers State University [8] using special many-body potentials such as Stillinger–Weber potential [9], Tersoff potential [10], and the modified Born–Mayer–Huggins (BMH) pair potential including Stillinger–Weber angular terms for covalent bondings and embedded atomic potentials (EAM) for metals [11].

3. Ag particles in glass and HREM imaging

Commercial sodium silicate glasses (0.13% Fe_2O_3) are exposed to an ion exchange in an $NaNO_3$–$AgNO_3$ melt at 400 °C. Subsequent annealing at temperatures between 460 and 600 °C creates Ag particles of up to 120 nm in size. Fig. 1(a) shows an experimental HREM micrograph of a silver particle within sodium silicate

[1] Permanent address: A.F. Ioffe Physico-Technical Institute, Russian Academy of Sciences, 19402 St. Petersburg, Russia.

0921-5107/96/$15.00 © 1996 — Elsevier Science S.A. All rights reserved
SSDI 0921-5107(95)01464-0

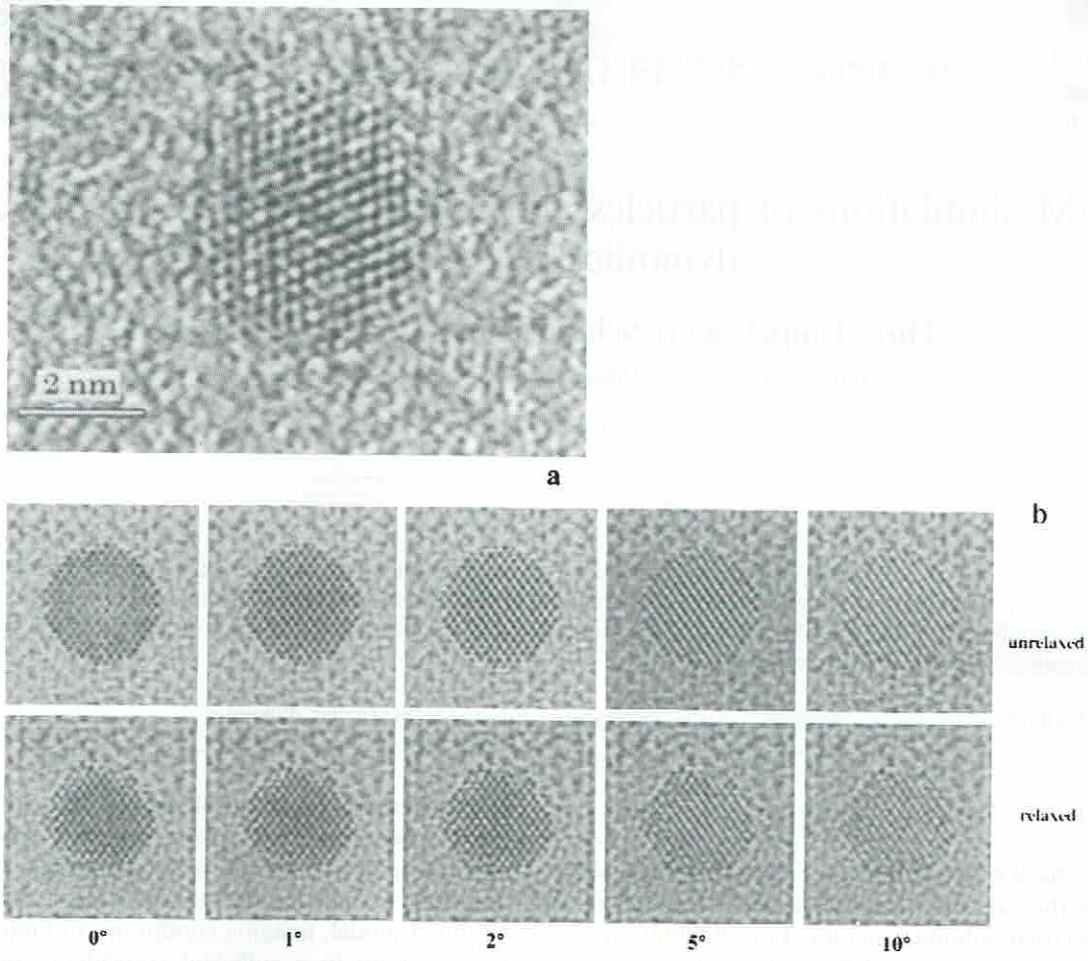

Fig. 1. (a) (111)-lattice fringes of an Ag-particle within commercial sodium silicate glass after ion exchange and annealing: $U = 400$ kV. (b) Calculated HREM micrographs of a spherical (011)-oriented Ag-particle (1722 atoms) before and after relaxation; particle is turned around $[1\bar{1}1]$ by rotation angle 0–10°. Imaging parameters: $U = 400$ kV; $C_s = 1$ mm; $\delta = 10$ nm; $\alpha = 0.5$ mrad; $\Delta = -37$ nm.

glass. The particles are investigated under lattice fringe imaging conditions using a JEOL-JEM 4000 EX electron microscope near the Scherzer focus. The (111) lattice fringes characterizing the crystalline particle structure clearly stand out against the speckled contrast of the amorphous matrix. Measurements of the fringe distances in experimental HREM micrographs indicate that with declining particle diameter the lattice parameters decrease more strongly than expected for free particles [12]. Based on structural models (see Fig. 2) computer simulated HREM images of both an unrelaxed and a relaxed spherical silver particle were calculated for the underfocus of -37 nm and for different orientations (see Fig. 1(b): acceleration voltage $U = 400$ kV; spherical aberration $C_s = 1$ mm; defocus spread $\delta = 10$ nm; semi-angular beam divergence $\alpha = 0.5$ mrad; diffraction aperture $\alpha' = 16$ nm^{-1}). Starting off in an (011) orientation, the particle is turned around $[1\bar{1}1]$ up to 10°. With increasing rotation angle the image contrast of the particle will be disturbed, but even at rotation angles up to 10° the lattice fringes of the precipitate can clearly be detected. The contrast of the relaxed particle seems to be less extended than that of the unrelaxed one, and is characterized by reduced lattice distances, indicating the compression of the particle as the result of MD relaxation.

4. Glass generation by MD simulations

In order to establish a realistic glass model, the MD relaxations should result in an amorphous structure having a local atomic environment similar to that of a crystal, considering the correlation of the atomic positions vanishing over far distances, and special topological rules. Different strategies of glass generation were checked. Starting from a $-Na_2Si_2O_5$ crystal, space group *Pcnb*, (Fig. 3(a)) either the crystalline atomic positions were statistically disturbed or the bonding relations were rearranged by converting some of the six-fold Si–O rings to five-, and seven-fold rings. Subsequent energy minimization yields a relaxed glass structure. Fig. 3(b) shows a glass structure modelled by MD simulations using BMH and EAM potentials after ran-

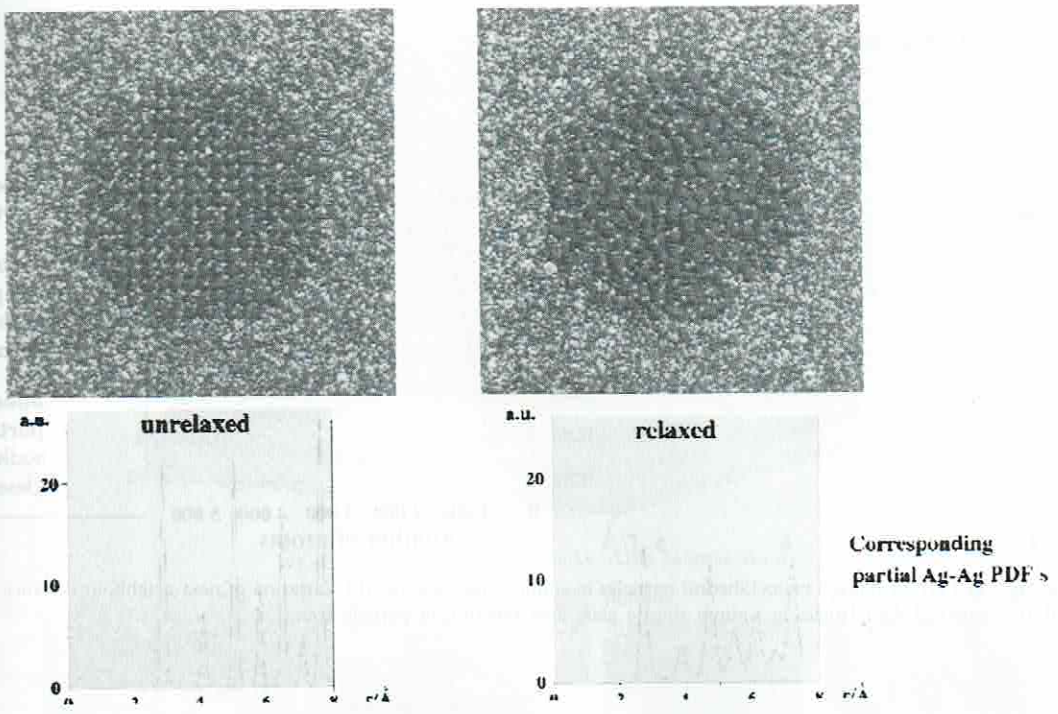

Fig. 2. Cuboctahedral Ag-particle in the $10 \times 4 \times 12$ supercell of the sodium silicate glass before and after relaxation: particle, 1290 atoms; supercell, $6.4 \times 6.2 \times 5.8$ nm.

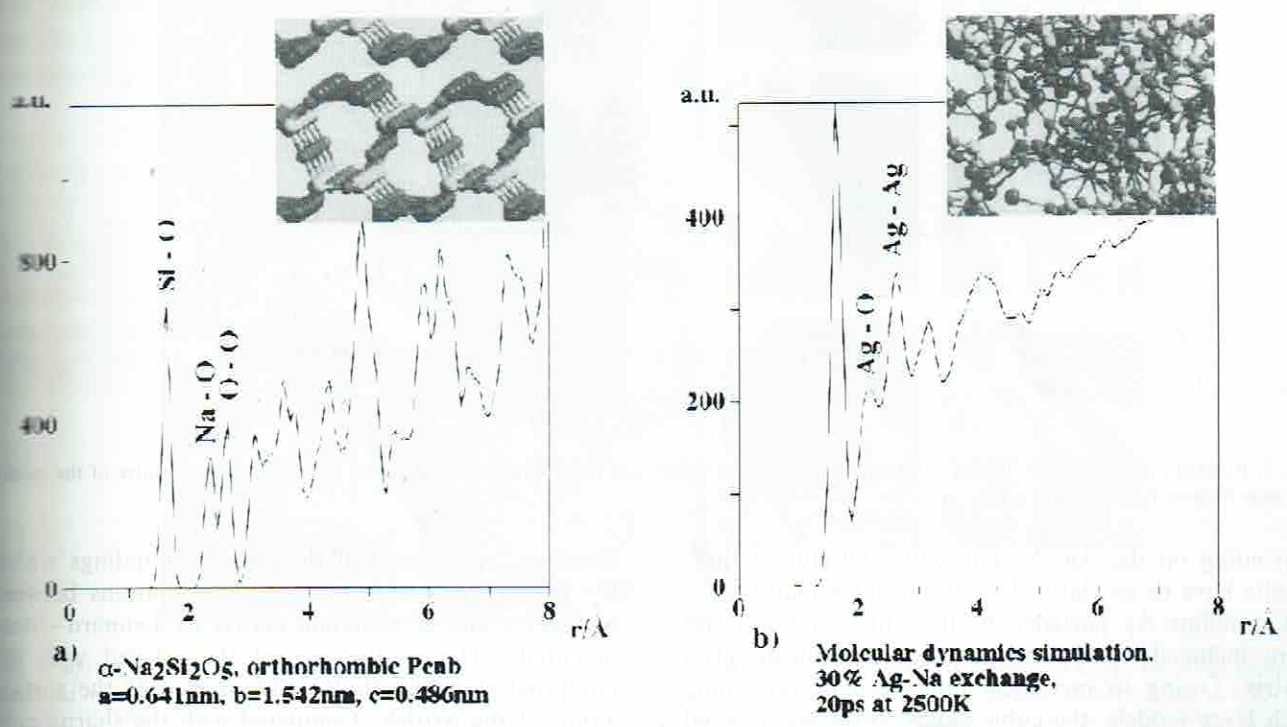

Fig. 3. Generation of sodium silicate glass models and corresponding PDFs.

domly replacing Na by Ag according to the experimental ion exchange rate. The glass was heated up to 2500 K in 20 ps. The corresponding pair distribution function (PDF) sufficiently describes the averaged local atomic environment and the long-range disorder. Compared with the peaks of the crystal, those of the glass structures are lowered and broadened. Solely for small distances, these structures reveal a correlation of the atomic position. In addition, the PDFs of the glass structures have Ag–Ag and Ag–O peaks. The annealing process of the ion-exchanged glass structure seems to cause a clustering of the Ag particles. However,

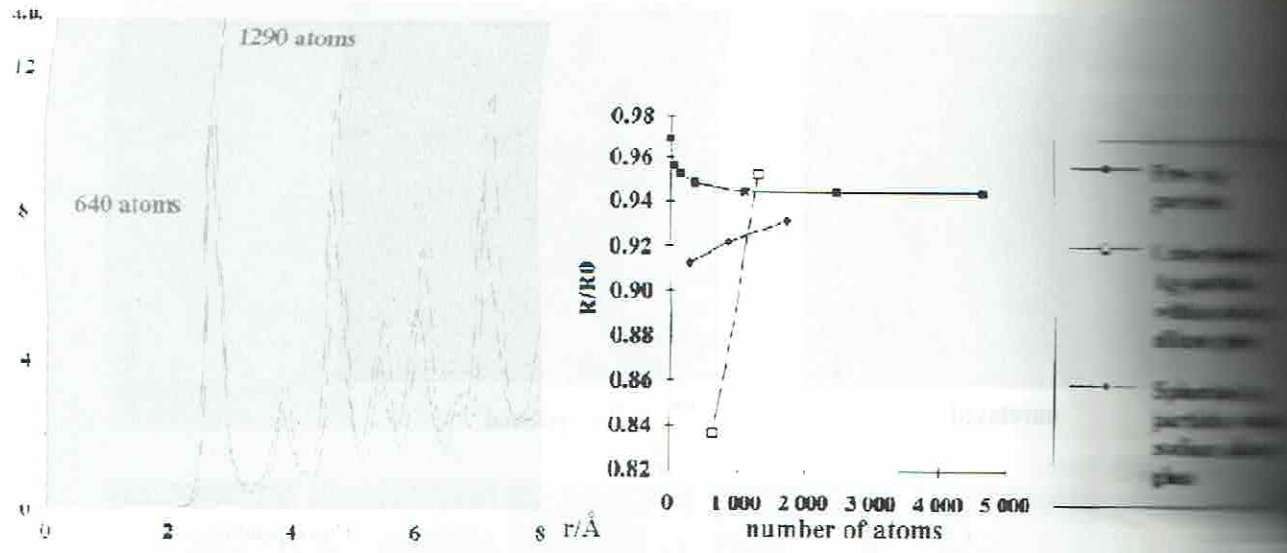

Fig. 4. (a) Partial Ag–Ag PDF of relaxed cuboctahedral particles in sodium silicate glass. (b) Variation of next-neighbour distance as cuboctahedral and spherical Ag-particles in sodium silicate glass as a function of particle size.

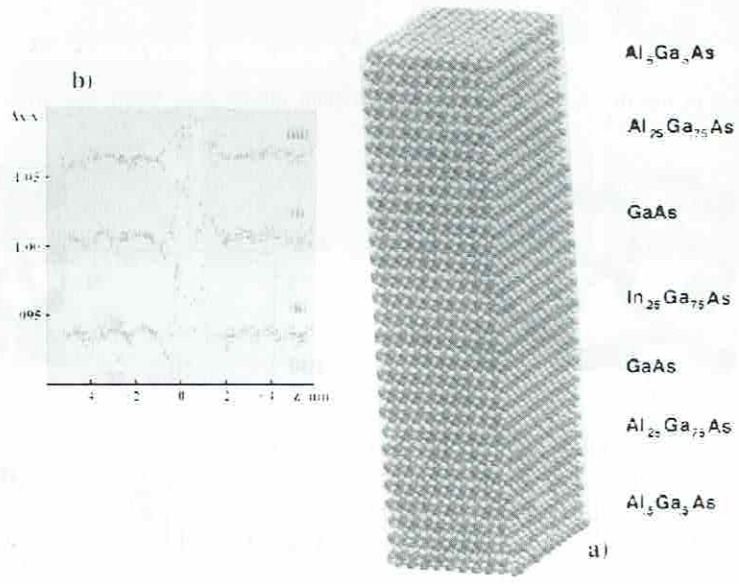

Fig. 5. Relaxed model of (a) an InGaAs–AlGaAs–GaAs QW structure and (b) strains measured across the QW at (i) the centre of the (ii) near the exit face, and (iii) a side face.

depending on the Ag–Ag pair potential chosen these results have to be clarified by future investigations.

Crystalline Ag particles of different shape and size were included in the enlarged sodium silicate glass matrix. Owing to numerical difficulties in generating such large models, the cubic glass matrix was created by statistically disturbing an enlarged crystal ($10 \times 4 \times 12$), recalculating the bonding relations, and subsequent energy minimization. Fig. 2 shows such a model including a spherical Ag particle (a) before and (b) after relaxation of the whole system, as well as the corresponding partial Ag–Ag PDFs. The energy was minimized by assuming a universal force field [5], which included pair and three-body interactions for the glass structure, and described the metallic bondings the particle as well as the bonding relations precipitate and surrounding matrix by Lennard– potentials. The comparison of the relaxed unrelaxed state reveals the disturbance of the atoms of the particle. Compared with the sharp of the unrelaxed precipitate, the peaks of the precipitate are lowered and broadened. Comparing partial Ag–Ag PDF of two embedded spherical particles of different size (640 and 1290 atoms) relaxation provides more detailed information relaxation behaviour of the precipitate (see Fig. For the smaller particle, besides a lowering broadening of the crystal peaks, there is a slight

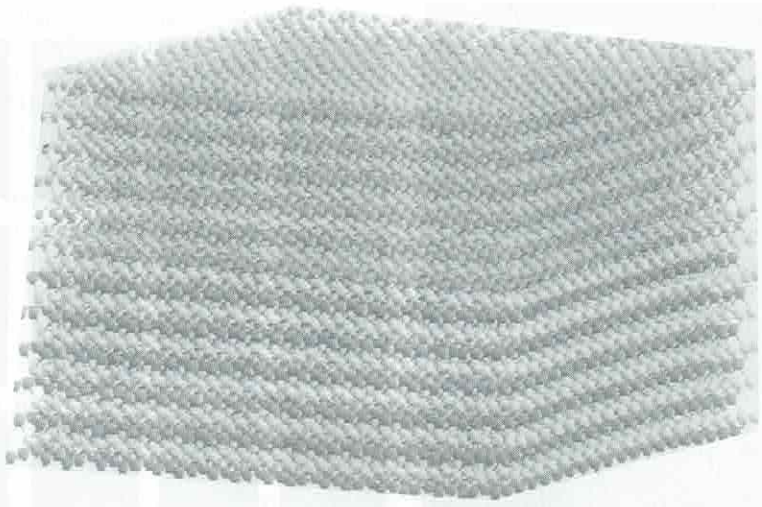

Fig. 6. Relaxed model of an InAs–AlSb heterostructure.

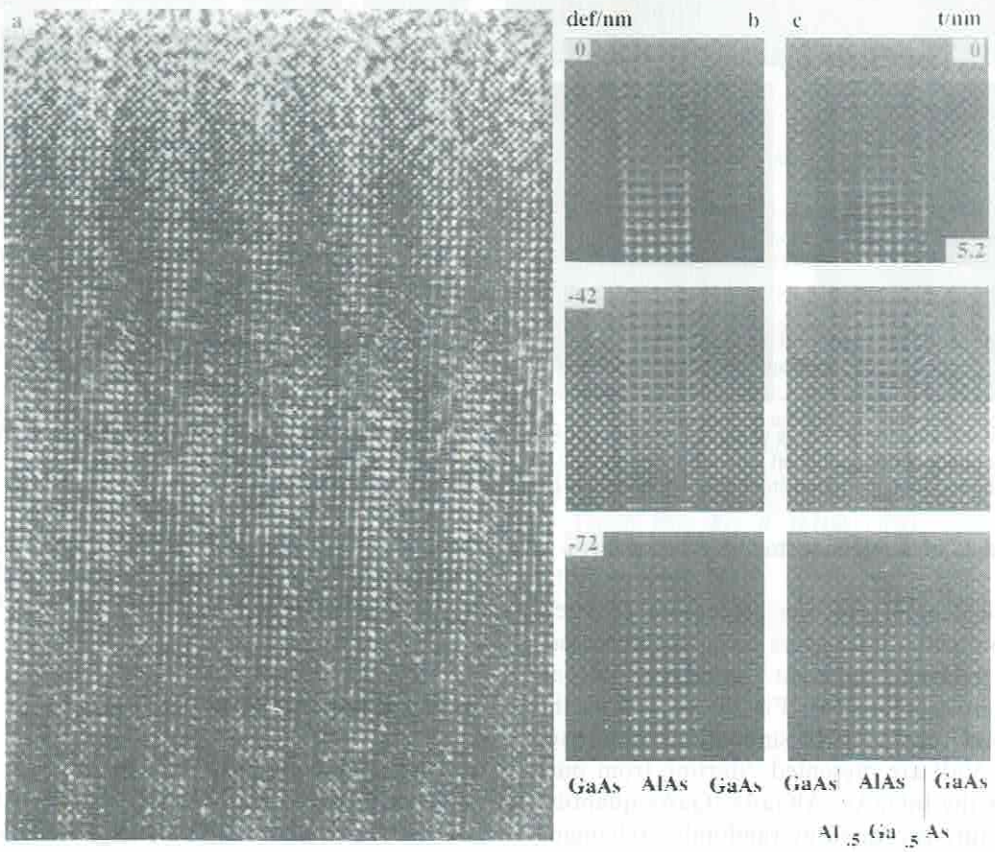

Fig. 7. 400 kV (110)-HREM image of (a) a (1.2 nm GaAs–1.2 nm AlSb)$_n$ QW structure grown on (001)-oriented GaAS by MBE; computer simulated images of an extended AlAs layer inserted in a 90° wedge-shaped GaAs matrix of thickness $t = 0.25$ nm. (b) Abrupt interface, (c) with $Al_{0.5}Ga_{0.5}As$ interlayers at both surfaces. Imaging parameters: $U = 400$ kV; $C_s = 1$ mm; $\delta = 8$ nm; $\alpha = 0.5$ mrad; $\Delta = 0, -42, -72$ nm.

the peak maxima towards the smaller distances. Fig. 4(b) summarizes the results for cuboctahedral and spherical precipitates embedded in two slightly different glass models, as well as for free particles of different size. For free particles, which are relaxed by using potentials and parameters equivalent to those of embedded ones, the next neighbour distances increase with decreasing particle size. In contradiction to the experiments, it demonstrates Lennard–Jones potentials being insufficient for metals. Nevertheless, the embedded particles show an opposite behaviour: the obvious influence of the matrix results in an additional pressure on the particle.

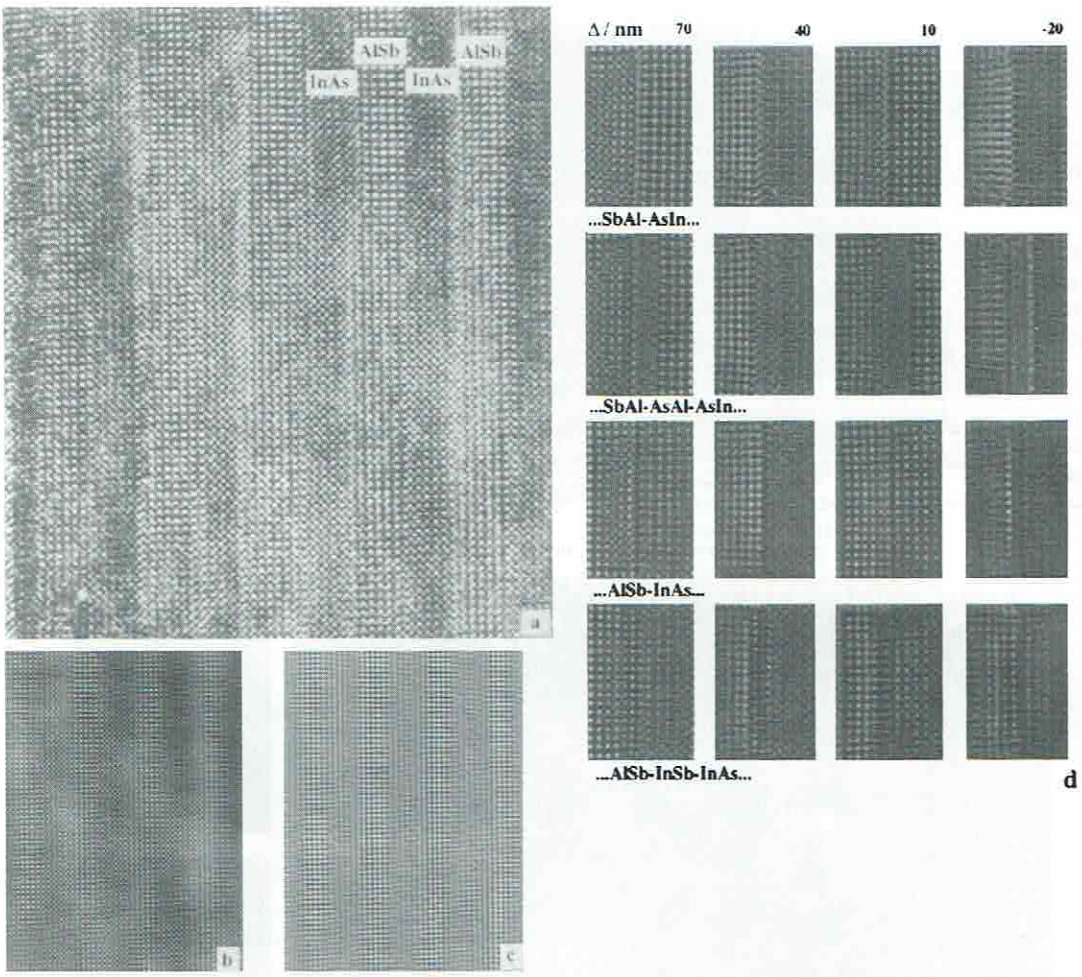

Fig. 8. Experimental 400 kV HREM image of (a) (1.8 nm InAs–1.8 nm AlSb)$_n$ multi-layer structure; (b) sections filtered with 35 beams; (c) {200} beams. (d) Simulated images using different defoci for four atomic sequences across the InAs–AlSb interface (Al–As or In–As interface with an AsAl or InSb interlayer). Imaging parameters: $U = 400$ kV; $C_s = 1$ mm; $\delta = 8$ nm; $\alpha = 0.5$ mrad; $t = 11.3$ nm; $\Delta = 70, 40, 10, -10$ nm.

5. Interface models of semiconductor heterostructures

Figs. 5 and 6 demonstrate the generation of interfaces in semiconducting interlayers using atomistic calculations. A relaxed coherent interface of an InAs–AlSb heterostructure (see Fig. 6) as well as the basic model used for the MD simulation of ternary structures (Fig. 5(a)) are presented. Starting from pure GaAs supercells the InGaAs–AlGaAs–GaAs quantum well (QW) structure is created by randomly exchanging In and/or Al atoms for Ga in different layers. The latter are matched, with the bonds being recalculated before the energy is minimized by using a force field, with the atomic distances varying. The misfit is determined by the different equilibrium interatomic distances, chosen to get stable crystal structures. The misfit varies between 0.1% for AlAs–GaAs and 1.2% for InAs–AlSb. Strain measurements across the QW (Fig. 5(c)) visualize the results of relaxation. The QW structures are studied to analyse the different factors influencing the HREM contrast at the interfaces. The systems are characterized by different misfits and scattering factors, resulting in a different elastic behaviour at the boundaries and in respective imaging effects.

6. Small interface misfit multi-layers

Fig. 7(a) compares an experimental (110)-HREM image (a) of a (1.2nm GaAs–1.2nm AlAs)$_n$ QW grown on (001)-oriented GaAs by MBE to computer-simulated images of an extended AlAs layer inserted in a 90° wedge-shaped GaAs matrix. According to the dynamical scattering theory, the thickness contours and related contrast shifts are visualized in the experimental images. The micrographs were computed by assuming an abrupt interface (Fig. 7(b)) as well as $Al_{0.5}Ga_{0.5}As$ interlayers at both interfaces (Fig. 7(c)). Respective computer simulations applied $U = 400$ kV, $C_s = 1$ mm, $\delta = 8$ nm, $\alpha_D = 0.5$ mrad, and $\alpha = 16$ nm^{-1}. Owing to the wedge-shaped model, in each simulated image the thickness increases from $t = 0$ to $t = 46$ nm. The defo-

cus values are 0, −42, and −72 nm. The small scattering factor asymmetry for GaAs (0.03) is opposite to the strong asymmetry in the AlAs (0.43) interlayer, thus explaining the different HREM patterns and the different defocus/thickness behaviour. This system has the lowest misfit considered, with no additional contrast modifications and no streaks occurring at the interfaces. The graduated interlayer (Fig. 7(c)) is the sole cause of the abrupt contrast change smoothing down, but causes no additional features.

7. Large interface misfit multi-layers

The InAs–AlSb system (model, see Fig. 6(b)) is characterized by a large misfit and a structure factor asymmetry as well as by two very different interfaces. Fig. 8(a) shows an experimental HREM micrograph of the InAs–AlSb multi-layer system and its contrast enhancement by Fourier processing using 35 beams (Fig. 8(b)) or solely the {200} reflections (Fig. 8(c)). In analysing the micrograph one can detect the layer sequence (InSb and AlAs interface) and the roughness of the interfaces (steps). The latter are no longer abrupt. Local variations of the orientation create virtual boundary structures, which cannot be analysed in a phenomenological manner. In some places finer fringes occur, which can be interpreted as 'half spacings'. The simulated defocus series using underfocus values of 70, 40, 10 nm and an overfocus value of −20 nm are shown in Fig. 8(d). In most cases the different layers can clearly be distinguished and their atomic columns or pairs can be directly imaged. Interface delocalization and visibility show maxima at an overfocus of 40 nm. Varying the defocus may change the orientation of the striations according to the strains. Such features are less pronounced in the experimental images than in the simulated ones considering the relaxation, which were calculated by energy minimization of the structure including the misfit. Thus MD calculations require better boundary conditions, larger atomic numbers in simulations, and potential refinements for a more quantitative image matching. The different assumptions of the local interface structure in the InAs–AlSb system imply different contrasts at the boundaries where the interface region is blurred and extended if additional interlayers are considered.

Acknowledgements

The authors are very thankful to H. Hofmeister (MPI Halle), M. Dubiel and K.-J. Berg (Martin Luther University of Halle) for cooperation and discussion, and to the DFG and Stiftung Volkswagenwerk for financial support.

References

[1] K.-J. Berg, A. Berger and H. Hofmeister, *Z. Phys. D, 20* (1991) 313.
[2] K. Scheerschmidt and D. Timpel, *Optik, 93* (Suppl. 5) (1993) 81.
[3] K. Scheerschmidt and D. Timpel, *Electron Microscopy: Proc. 13*, Vol. 2A, ICEM, Paris, 1994, p. 395.
[4] S. Ruvimov et al., *Electron Microscopy: Proc. 13*, Vol. 1, ICEM, Paris, 1994, p. 403.
[5] K. Scheerschmidt, in P. Borgesen et al. (eds.), *Proc. MRS 1994 Spring Meeting, San Francisco*, Vol. 338, p. 121
[6] K. Scheerschmidt et al., *J. Microsc., 179* (1995) 214.
[7] CERIUS a program package for MD calculation, (Molecular Simulations, Inc., Cambridge, UK).
[8] S.H. Garofalini, *J. Non-Cryst. Solids, 120* (1990) 1.
[9] F.H. Stillinger and T.A. Weber, *Phys. Rev. B, 31* (1985) 5262.
[10] J. Tersoff, *Phys. Rev. B, 37* (1988) 6991.
[11] G.J. Ackland, G. Tichy, V. Vitek and M.W. Finnis, *Philos. Mag. A, 56* (6) (1987) 735.
[12] S. Giorgio and J. Urban, *J. Phys. F:*, 18 (1988) 147.